

# Fluid flow through a vertical to horizontal 90° elbow bend III three phase flow

P.L. Spedding, E. Benard \*, N.M. Crawford

*School of Mechanical and Aerospace Engineering, Queen's University Belfast, Ashby Building, Belfast BT9 5AH, United Kingdom*

## Abstract

Three phase water/oil/air flow was studied around a vertical upward to horizontal 90° elbow bend of  $R/d = 0.654$ . The results were more complex than corresponding two phase data. The pressure drop recorded for the two tangent legs sometimes showed significant variations to the straight pipe data. In most cases this variation was caused by differences in the flow regimes between the two systems. The elbow bend tended to constrict the flow presented by the vertical inlet tangent leg while sometimes acting as a wave and droplet generator for the horizontal outlet tangent leg. It could be argued that the inclusion of the elbow bend altered the flow regime map transitional boundaries but it also is possible that insufficient settling length was provided in the apparatus design.

The elbow bend pressure drop was best presented as  $l_e/d$  the equivalent length to diameter ratio using the actual total pressure drop in the vertical inlet tangent leg. Generally  $l_e/d$  values rose with gas rate, but exhibited an increasingly complex relation with  $f_o$  the oil to liquid volumetric ratio as liquid rate was increased. A significant maximum in  $l_e/d$  was in evidence around the inversion from water dominated to oil dominated flows. Several models are presented to predict the data.

*Keywords:* Air–water–oil flow; Three phase flow in bend; Bend pressure loss; Prediction of pressure loss

## 1. Introduction

Generally three phase flow is more complex than the corresponding two phase gas liquid flow because an additional variable is involved namely  $f_o$  the oil to liquid volumetric ratio. The flow can be oil dominated (OD), water dominated (WD) or in the transitional region in between where a large increase in viscosity takes place. A review on three phase oil, water, gas flow in horizontal pipes has recently appeared [1]. Early work on three phase horizontal flow was unsystematic and useful data were limited [2–6]. Much of the following work emphasised the conditions, such as settling lengths, necessary to achieve reliable data [7–11]. Flow regimes were also identified and flow pattern maps proposed [1,2,4,7–10,12–16]. Malinowsky [12] and

Laffin and Oglesby [13] conducted three phase experiments in 0.038 m i.d. horizontal pipe. The main focus was to attempt to determine an effective liquid viscosity using correlations developed from the phase liquid systems. Fayed and Otten [17] extended the approach. Others such as Stapelberg and Mewes [7,8] and Taitel et al. [18] attempted to extend two phase flow models to the three phase system, while Hall [19] and co-workers [16] attempted to extend other models to the three phase situation. Spedding et al. [20] have shown that two phase correlations extended to three phase were only successful in prediction of intermittent slug type flows in certain cases.

By contrast with the horizontal case relatively little has been published on three phase flow in vertical pipe. Early fieldwork [21–23] lacked detail to be of real value. Shean [24] and Pleshko and Sharma [25] obtained scattered data on 0.0109 m i.d. and 0.051 m i.d. pipe respectively. Any attempt to adapt the three phase data obtained to modified

\* Corresponding author. Tel.: +44 1413302530; fax: +44 1413305560.  
E-mail address: [ebenard@aero.gla.ac.uk](mailto:ebenard@aero.gla.ac.uk) (E. Benard).

## Nomenclature

$d$	internal diameter (m)
$f_o$	oil to liquid volumetric ratio
$l_e$	equivalent length (m)
$P$	pressure ( $\text{kg m}^{-1} \text{s}^{-2}$ )
$R$	elbow bend centre line radius (m)
$t_o$	temperature ( $^{\circ}\text{C}$ )
$X$	Lockhart–Martinelli parameter
$\rho$	density ( $\text{kg m}^{-3}$ )
$\mu$	viscosity ( $\text{kg m}^{-1} \text{s}^{-1}$ )
$\sigma$	surface tension ( $\text{kg s}^{-2}$ )
$\varphi$	Lockhart–Martinelli parameter

## Subscripts

A	air
B	bend
G	gas
L	liquid
O	oil
S	superficial
T	total
W	water

two phase models proved to be unsuccessful. Chen et al. [26] also reported on vertical three phase flow. Woods et al. [27,28] has presented detailed descriptions of the three phase flow regimes found in vertical flow together with pressure drop and holdup data. A method for prediction of holdup was also given.

Ito [29] provided a definitive appraisal of single phase pressure drop in curved pipe. Later Crawford et al. [30] extended the development to elbow bends. Recent work on two phase flow in elbow bends [31] demonstrated that the pressure drop can be successfully correlated by using a Lockhart–Martinelli [32] type parameter based on the single phase bend pressure drop [33]. There is no reported work on three phase pressure drop in elbow bends. This work is concerned with the pressure drop of three phase air, water and oil flow through a vertical to horizontal  $90^{\circ}$  elbow bend with a  $R/d$  value of 0.654. It is an extension of single phase [33] and two phase work [31] conducted on the same apparatus.

## 2. Experimental

Fig. 1a is a schematic diagram of the main section of the rig. It was made of clear Perspex 0.026 m i.d. pipe. Individual lengths were flanged, gasketed and bolted together and exactly matched the pipe internal diameter. Detail of the elbow bend are given in Fig. 1b which is a standard PV fitting and again exactly matched the inner pipe surface. The  $X$  section of the apparatus was set vertical while the  $Z$  section was horizontal. The whole rig was rigidly supported. All dimensions shown on Fig. 1a are in meters. Tapping points were set into the side of the vertical pipe and on the top of the horizontal section. Each tapping point consisted of a clear Perspex tube 0.003 m i.d., 0.005 m o.d. and 0.020 m long set into the pipe wall flush with the internal surface. Each tapping point was connected by a short PVC tube to the side of an enclosed cylindrical separator cup 0.026 m i.d. and 0.085 m in height. These cups ensured that the pressure measuring line from the cup top to the manometer were

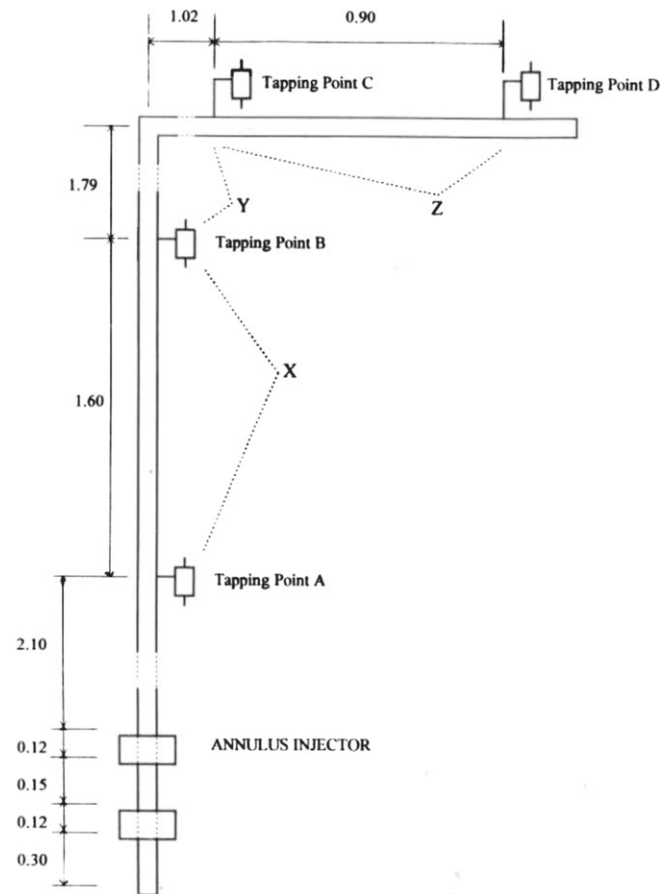


Fig. 1a. Schematic diagram of apparatus. Lengths are shown in meters.

liquid free. The bottom drain from the cup was sealed. Actually the liquid height in the cup reflected the total liquid holdup in the main pipe at that location. What is not shown in Fig. 1a are a series of tapping points 0.1 m apart set along the total pipe length from the top annulus injector. These tapping points were used to validate the rig and then sealed. The pressure drop in the rig was measured by an Air Neotronics Zephyr D.P. data logger of  $\pm 1\%$  accuracy which gave the average pressure

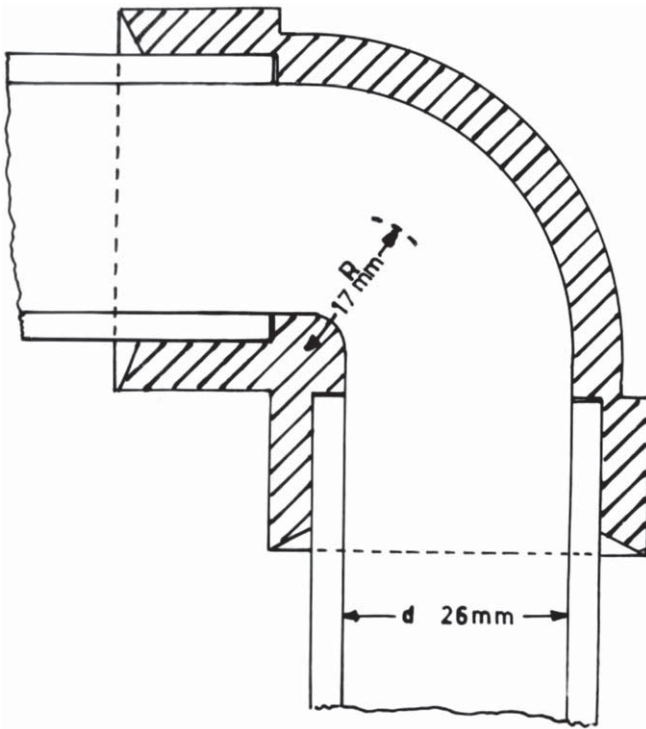


Fig. 1b. The elbow bend.

difference and the maximum and minimum readings. At least three consistent results were taken for each reading. The air was drawn from compressors, the flow measured and passed into the base of the inlet tangent leg *X*. Water and oil were then injected into the flow through the lower and upper annular injectors respectively. These consisted of an annular pipe, set around the main pipe, 0.12 m long and 0.074 m i.d. sealed at both ends with three tangential entrances for the liquid. The inner wall of the annulus was perforated by a series of fine holes through which the liquid passed into the gas flow as a spray creating intensive mixing of the fluid phases. The liquids were drawn from their respective storage vessels by individual centrifugal pumps, metered in calibrated rotameters and passed to the respective annulus injectors. Exiting fluids from the horizontal section *Z* were sent to a cyclone air liquid separator which prevented back pressure reflection. The liquids were sent to a liquid separator and then to storage for recycling. The flow rates used were up to  $0.02 \text{ m}^3 \text{ s}^{-1}$  for air,  $0.00015 \text{ m}^3 \text{ s}^{-1}$  for water and  $0.0001 \text{ m}^3 \text{ s}^{-1}$  for oil. Flow control was achieved by valve adjustment and bypass systems. Readings were taken at set gas and total liquid rates and for  $f_o$  values of varying from 0 to 1.0 and back from 1.0 to 0. The oil employed was Fina Vestan A 50 B of the following physical properties.

Density	$\rho_o = 832.5 + [0.7(15 - t_o)] \text{ kg m}^{-3}$
Viscosity	$\mu_o = 0.0203275 - 0.0004151 t_o \text{ kg m}^{-1} \text{ s}^{-1}$
Surface tension	$\sigma_{o-A} = 0.0305 \text{ at } 20^\circ \text{C kg s}^{-2}$
	$\sigma_{o-W} = 0.0315 \text{ at } 20^\circ \text{C kg s}^{-2}$

### 3. Preliminaries

Preliminary experiments were conducted on single phase air flow [33] and air water two phase flow [31]. Also three phase studies were conducted in vertical pipe [27,28] and horizontal pipe [1] of the same diameter. This allows checks to be made on the vertical riser *X* and the horizontal outlet *Z*. Detailed checks on the pressure drop profiles using the tapping points set at 0.1 m intervals over the whole pipe enabled settling and recovery lengths over the elbow bend to be determined. The pressure drop in the inlet leg was the total, ie. the friction plus head pressures. The total elbow bend pressure drop in the *Y* region,  $\Delta P_{BT}$ , was determined as the difference between the pressure drop in each leg *X* and *Z* extended to the elbow bend plus an equivalent pressure drop for the centre line length of the bend. Fig. 2 outlines the calculation. A–C and D–F are the actual up and downstream pipe tangential lengths, C–D is the elbow bend total centre line length, B–C and D–E are the up and downstream transitional regions. The point G is the demarcation between the straight pipe pressure drop of the two tangents which was chosen, not half way at the  $45^\circ$  line but at the  $90^\circ$  intersection where gravity effects in the vertical tangent cease. The actual pressure distribution in Fig. 2 is a b c g d e f, while the straight pipe distribution in the two tangent legs are a b c<sup>1</sup> g<sup>1</sup> and g<sup>1</sup> d<sup>1</sup> e<sup>1</sup> f<sup>1</sup>. The corrected pressure distribution from which the bend pressure loss is calculated is a b c<sup>1</sup> g<sup>11</sup> d<sup>111</sup> e<sup>111</sup> f<sup>111</sup> and includes a straight pipe loss equal to the actual length C–D of the elbow bend centreline, registered as  $\Delta P_{BE}$ , that is composed of C–G and G–D the two elements from each tangent leg. The method of presentation given in Fig. 2 was devised by Ito [29] and is generally accepted in the field since it separates to the right of the diagram the actual bend pressure drops so removing them from the actual bend area. The primed designations indicate that the values were lifted vertically while the double primes indicate the values were moved horizontally to the right to incorporate the equivalent effect of flow round the inside of the bend. The readings were taken for set air and total liquid rate with increasing and then decreasing  $f_o$  values. The holdup was determined in regions *X* and *Z* by means of quick closing valves not shown in Fig. 1aa. Generally, with three phase flow the procedure necessary to obtain reliable results is much more complex than with two phase flow. Two examples suffice. For three phase holdup measurement the estimation of liquid resident on the pipe wall after draining of that between the cut off valves needed to be calculated for each value of  $f_o$  in the feed. Secondly, the time effect outlined by Woods et al. [27] meant that at least 30 min running of the flow was required before consistent readings were obtained. The flow regimes were identified by a combination of visual observation, imaging, holdup and the pressure drop profile. Visual observation was best achieved by viewing out of the corner of the eye at a

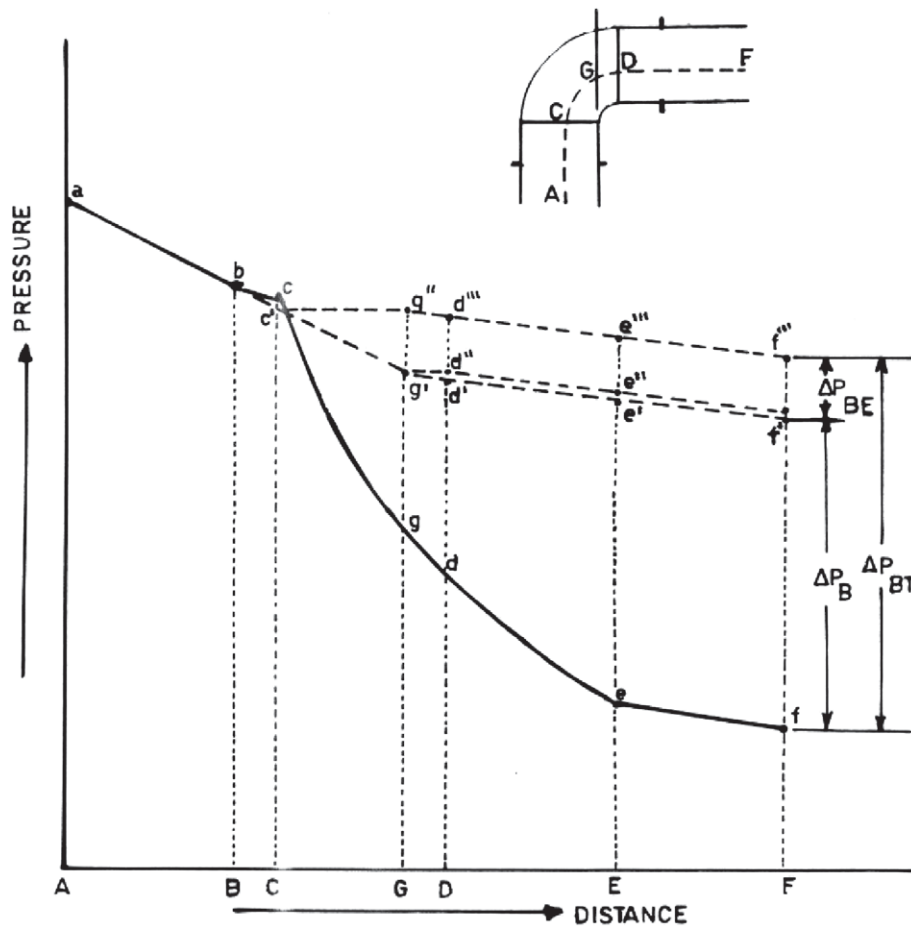


Fig. 2. Schematic diagram of the three phase pressure loss in a horizontal to vertical 90° elbow bend.

sharp angle to the flow. The regimes are detailed in Appendix. Further, details of experimental method and results are presented elsewhere [34].

#### 4. Results

In general the results were more complex than for single and two phase flow. This was to be expected from an examination of corresponding data for straight pipe, and because another variable  $f_o$ , the oil to liquid volumetric ratio, was involved.

Figs. 3–11 outline the results obtained for the various pressure drops through both tangents and the elbow bend for a series of total liquid and gas rates. In the Figures the pressure loss is presented for straight vertical pipe (SVP) [28], the horizontal outlet tangent leg Z (OHTLZ), the elbow bend region Y (EBRY), and the elbow bend expressed in two ways, as total bend pressure loss  $\Delta P_{BT}$  and as  $l_e/d$  using the vertical inlet tangent leg X (VITLX) pressure loss. In some cases the data for the outlet leg Z are compared with the results of Donnelly [35] for three phase horizontal flow.

There was an observable difference in the vertical pipe result if the gas rate was below or above  $\bar{V}_{SG} = 10 \text{ m s}^{-1}$ .

The reason being that for  $\bar{V}_{SG} < 10 \text{ m s}^{-1}$  the semi-annular<sup>1</sup> regime (No 20) was present in the vertical inlet tangent leg X, where the pressure loss fell with increasing gas rate while for  $\bar{V}_{SG} > 10 \text{ m s}^{-1}$  the annular regime (No 17) was in evidence where the pressure loss rose with gas rate. Figs. 3, 6 and 9 give data for the lowest gas rate for increasing total liquid rate. Examining each of these three figures in order allows insight to be gained on the general processes involved. It should be noted that a qualitative explanation of the processes taking place in straight vertical pipe has been presented by Woods et al. [27,28] who examined the interplay of phase velocity, thickness and holdup on the flow regimes present in the system and their effect on pressure loss. In Fig. 3 the vertical inlet tangent leg X pressure loss passed through a minimum value at  $f_o = 0.3$  and rose to a maximum at  $f_o = 0.75$  following inversion to oil dominated flow. There was a slight dip in the relation at  $f_o = 0.625$  due to the tendency to form the water dominated water annulus/oil annular plus ripple flow regime (No 12) just before the system inverted to the oil dominated regime.

<sup>1</sup> Flow regimes are illustrated and numbered in Appendix.

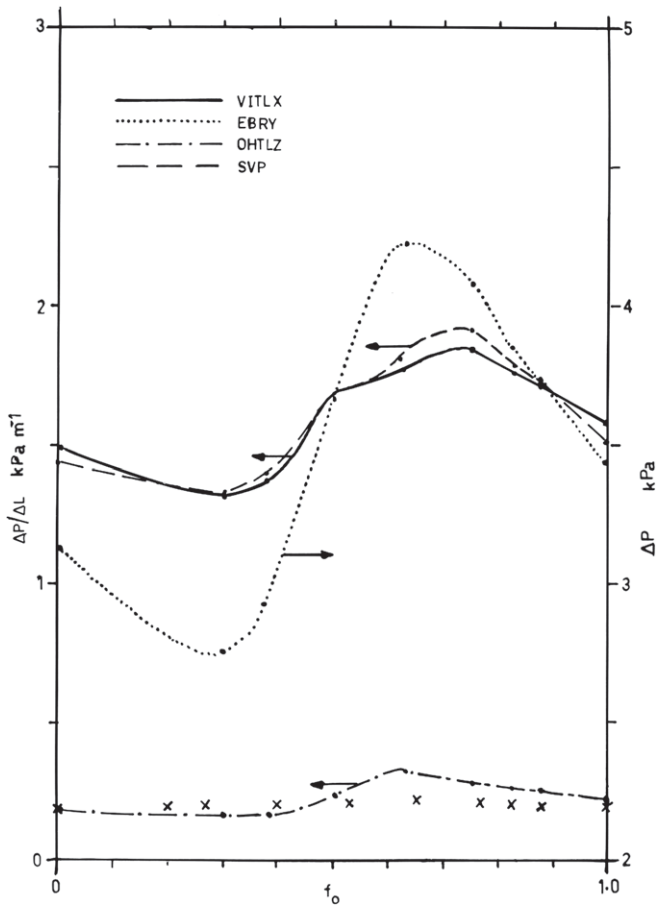


Fig. 3. Pressure losses through the vertical inlet tangent leg  $X$  (VITLX), straight vertical pipe (SVP), elbow bend region  $Y$  (EBRY), outlet horizontal tangent leg  $Z$  (OHTLZ), for  $\bar{V}_{SLT} = 0.0628 \text{ m s}^{-1}$  and  $\bar{V}_{SG} = 8.5 \text{ m s}^{-1}$ . X = Donnelly [35] data.

Other than this there was no discernible difference between the flow regimes for the vertical inlet tangent leg  $X$  and straight vertical pipe. In general the form of the pressure loss through the vertical inlet tangent leg  $X$  followed that for straight vertical pipe with a tendency to be above the straight vertical pipe values at the extremities of  $f_o = 0$  and  $f_o = 1.0$  and to be below the straight vertical pipe data in the intermediate region particularly at the maximum point at  $f_o = 0.75$  where the flow regime had passed from water dominated flows to the oil dominated dispersed semi-annular (No 5) pattern. The pressure drop fluctuated over a wider range in the vertical inlet tangent leg  $X$  than in the corresponding straight vertical pipe. At the  $f_o = 0.625$  point the flow regime fluctuated from water dominated dispersed semi-annular (No 20) to water dominated water annulus/oil annular plus ripple (No 12) flow while also beginning to show signs of starting to invert to oil dominated flow. It is of significance that the dip in the pressure drop relation at  $f_o = 0.625$  in Fig. 3 subsequently increased in intensity as the gas flow (c.f. Fig. 4) and the liquid flow (c.f. Fig. 6) were increased.

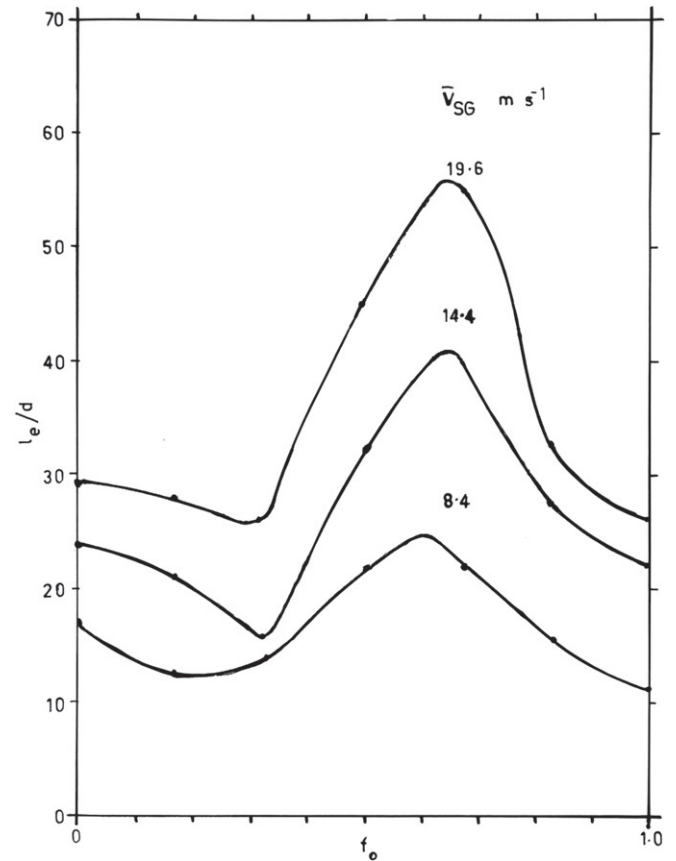


Fig. 3a. Bend pressure loss  $\Delta P_{BT}$  for  $\bar{V}_{SLT} = 0.0628 \text{ m s}^{-1}$  and various gas rates.

In Fig. 6 the total liquid velocity was double that of Fig. 3 for the same gas rate, and the pressure loss in the vertical inlet tangent leg  $X$  altered significantly from that for straight vertical pipe. The pressure loss in the vertical inlet tangent leg  $X$  was above that for straight vertical pipe at the extremities of  $f_o = 0$  and  $f_o = 1.0$ , (as also found in Fig. 3), and the dip in the relation at  $f_o = 0.625$  deepened as was previously mentioned, but on either side of this feature the vertical inlet tangent leg  $X$  values were significantly above those for straight vertical pipe. The reason was that there were differences in the flow regimes between the two systems. For straight vertical pipe at  $f_o = 0.5$  the flow regime present was water dominated dispersed semi-annular (No 20) flow while at  $f_o = 0.75$  it was oil dominated dispersed annular (No 2) flow. The corresponding vertical inlet tangent leg  $X$  regimes were water dominated dispersed semi-annular plus roll wave (No 22) and oil dominated dispersed semi-annular (No 5), respectively. Both these latter two regimes would have greater pressure drops than the respective straight vertical pipe patterns. It is apparent that the resistive pressure of the elbow bend following the vertical inlet tangent leg  $X$  resulted in changes in the flow patterns and consequently the multiphase characteristics of the flow in a manner similar to that reported for near vertical flow by Spedding et al. [28]. Secondly, the



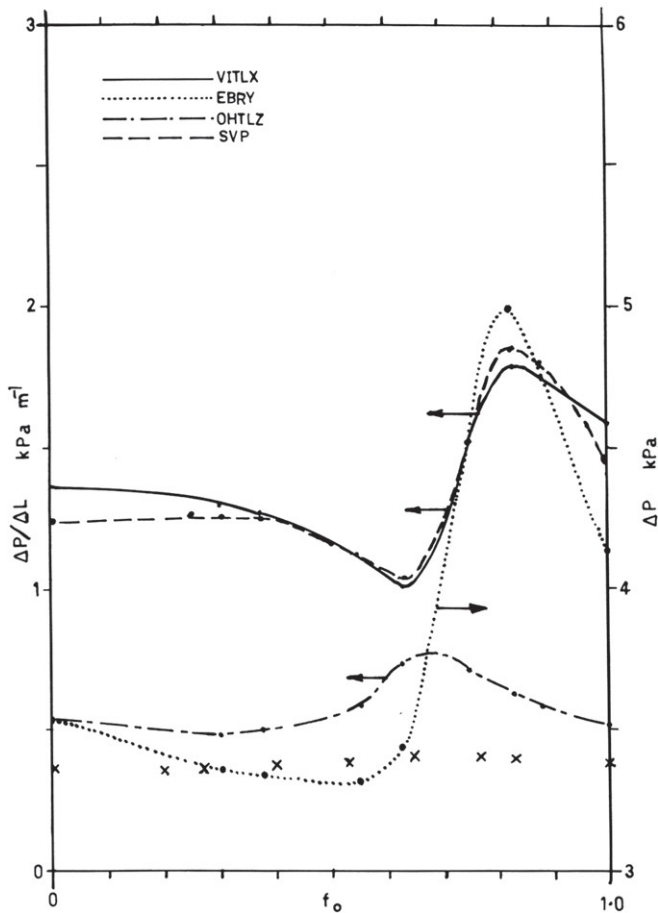


Fig. 4. Pressure losses through the vertical inlet tangent leg  $X$  (VITLX), straight vertical pipe (SVP), elbow bend region  $Y$  (EBRY), horizontal outlet tangent leg  $Z$  (OHTLZ), for  $\bar{V}_{SLT} = 0.0628 \text{ m s}^{-1}$  and  $\bar{V}_{SG} = 14.6 \text{ m s}^{-1}$ .  $X$  = Donnelly [35] data.

actual pressure and sometimes the pressure loss fluctuations increased in magnitude. These effects rose with gas rate for a set liquid rate. In Fig. 3 the volume of liquid presented to the elbow bend by and large passed smoothly through the horizontal outlet tangent leg  $Z$  with minimal disturbance. However, when the liquid rate was doubled, as in Fig. 6, a measure of choking of the liquid flow was in evidence and the liquid passage through the elbow bend was somewhat restricted, resulting in an increase in absolute pressure in the vertical inlet tangent leg  $X$  over the straight vertical pipe valve and disturbance of certain flow patterns.

In Fig. 9 at the highest liquid flow rate used at the same gas flow used in Figs. 3 and 6, the general form of the pressure drop relation was very different to that observed at the lower total liquid rates. In addition, the straight vertical pipe pressure drop was above that for the vertical inlet tangent leg  $X$  at the inversion point of  $f_o = 0.625$  but below in other regions. These effects again were caused by differences in the flow regimes. For example in Fig. 9 the slug flow pattern (No 26) was present around the inversion point, where as in Figs.

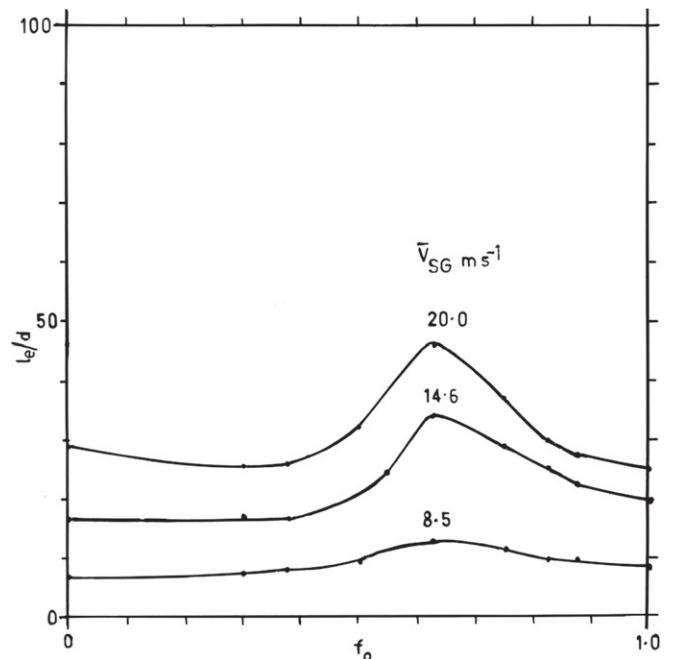


Fig. 4a. Bend pressure loss  $l_e/d$  for  $\bar{V}_{SLT} = 0.0628 \text{ m s}^{-1}$  and various gas rates.

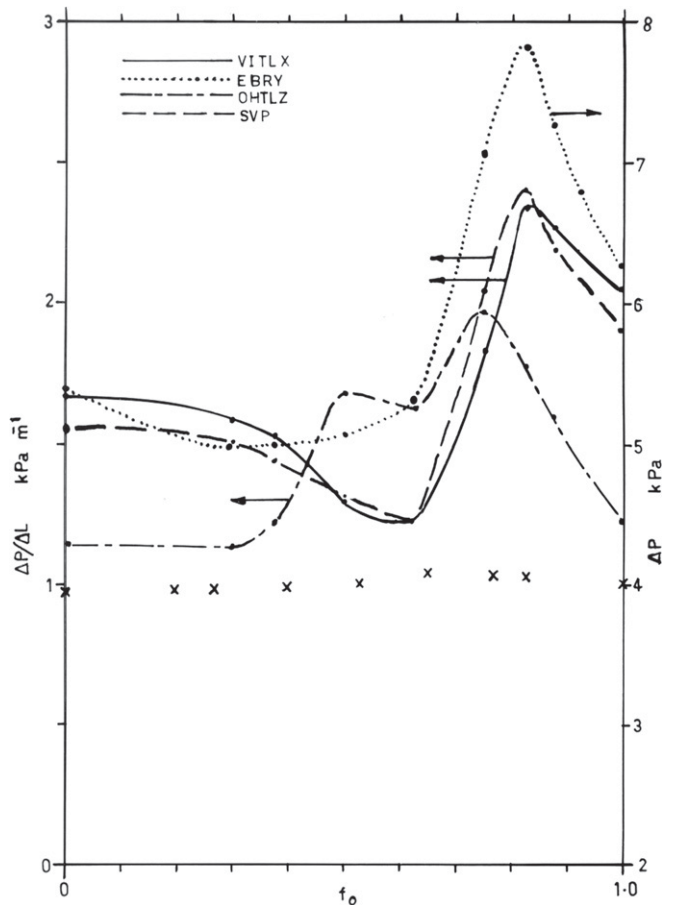


Fig. 5. Pressure losses through the vertical inlet tangent leg  $X$  (VITLX), straight vertical pipe (SVP), elbow bend region  $Y$  (EBRY), outlet horizontal tangent leg  $Z$  (OHTLZ), for  $\bar{V}_{SLT} = 0.0628 \text{ m s}^{-1}$  and  $\bar{V}_{SG} = 20.0 \text{ m s}^{-1}$ .  $X$  = Donnelly [35] data.

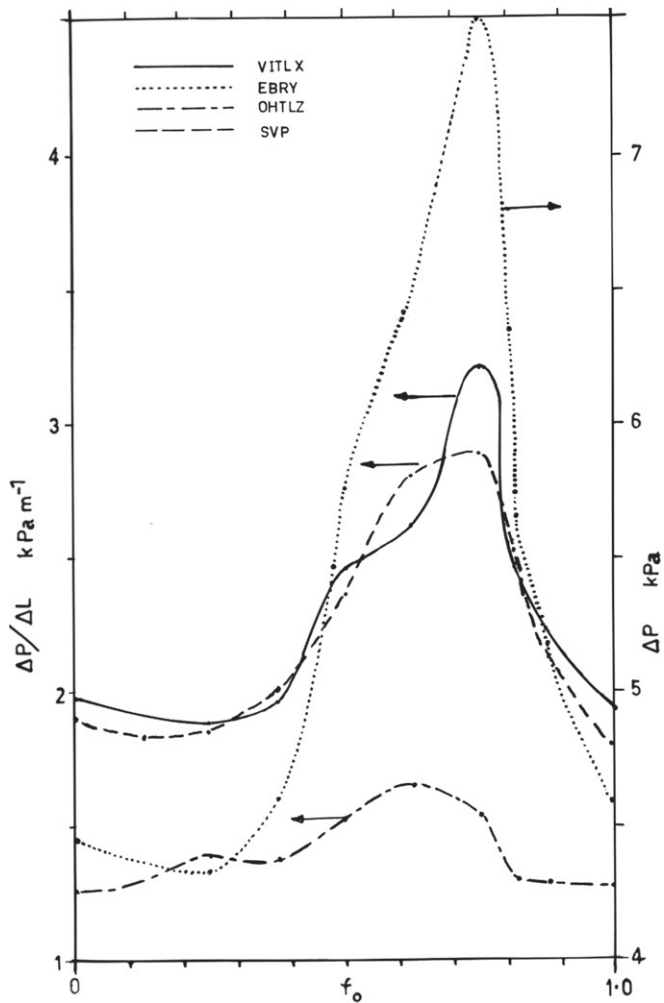


Fig. 6. Pressure losses through the vertical inlet tangent leg X (VITLX), straight vertical pipe (SVP), elbow bend region Y (EBRY), outlet horizontal tangent leg Z (OHTLZ) for  $\bar{V}_{SLT} = 0.1254 \text{ m s}^{-1}$  and  $\bar{V}_{SG} = 8.5 \text{ m s}^{-1}$ .

3 and 6, the dispersed semi-annular regime (No 20) was in evidence. In addition at  $f_o = 0.33$  in Fig. 9 the water dominated dispersed annular regime (No 17) was present in straight vertical pipe but in the vertical inlet tangent leg X the water dominated dispersed annular plus roll wave regime (No 19) was observed. Similarly near  $f_o = 1.0$  the oil dominated dispersed annular plus roll wave regime (No 4) was present in straight vertical pipe compared to the oil dominated dispersed slug regime (No 9) in the vertical inlet tangent leg X. There also was an observable difference in the slug length between the two systems. Thus a measure of choking of the liquid flow caused by the inclusion of the elbow bend resulted in changes in the flow patterns and the pressure drop in the vertical inlet tangent leg X fell below that for straight vertical pipe around the maximum point of  $f_o = 0.67$  while it was above in other regions.

The horizontal outward tangent leg Z data in Fig. 3 showed that the pressure drop maximised at  $f_o = 0.625$

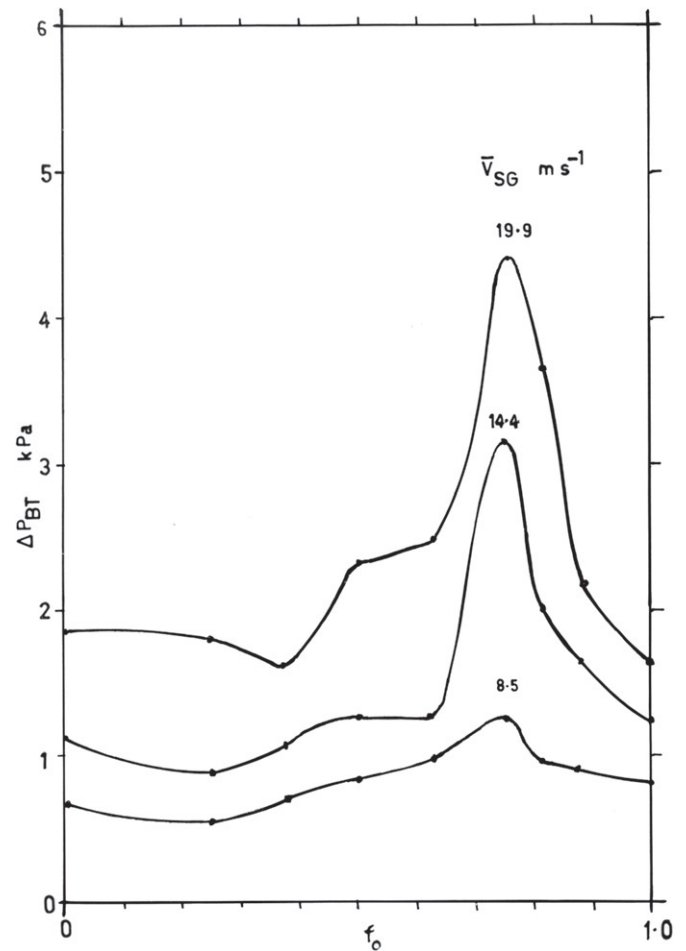


Fig. 6a. Bend pressure loss  $\Delta P_{BT}$  for  $\bar{V}_{SL} = 0.1254 \text{ m s}^{-1}$  and various gas rates.

in the water dominated region before inversion to oil dominated flow. The flow pattern passed from water dominated stratified plus ripple flow at  $f_o = 0.3-0.5$ , to water dominated stratified plus roll wave flow at  $f_o = 0.625$  before inverting to oil dominated stratified plus ripple flow at  $f_o = 0.75$ . Therefore, the maximum in the pressure drop at  $f_o = 0.625$  in Fig. 3 was due to the onset of roll waves on the liquid surface prior to inversion taking place in the horizontal outward tangent leg Z. The data of Donnelly [35] for 0.026 m i.d. horizontal pipe showed general agreement with the pressure drop obtained in this work except that the maximum point was lower in magnitude. Later work by Donnelly [35] for 0.05 m i.d. horizontal pipe exhibited a maximum pressure drop at  $f_o = 0.65$  that was more in agreement with this work.

As the liquid flow rate was doubled (in Fig. 6) the smooth transition through the elbow bend observed in Fig. 3 departed and waves were formed on the horizontal liquid surface which not only caused an increase in pressure drop in the horizontal outward tangent leg Z over that suggested by Donnelly [35] but a slight maximum

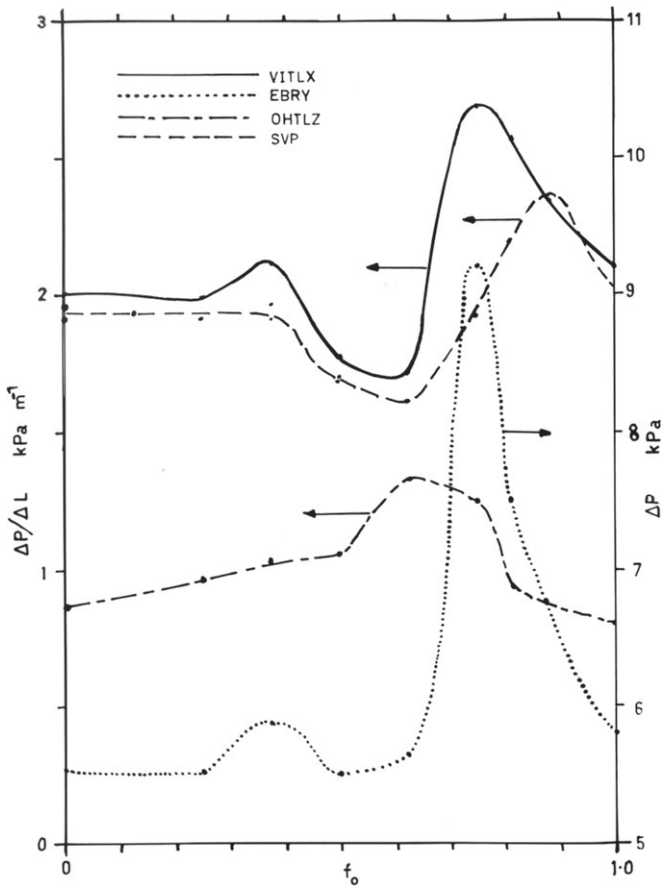


Fig. 7. Pressure losses through the vertical inlet tangent leg  $X$  (VITLX), straight vertical pipe (SVP), elbow bend region  $Y$  (EBRY), outlet horizontal tangent leg  $Z$  (OHTLZ) for  $\bar{V}_{SLT} = 0.1254 \text{ m s}^{-1}$  and  $\bar{V}_{SG} = 14.4 \text{ m s}^{-1}$ .

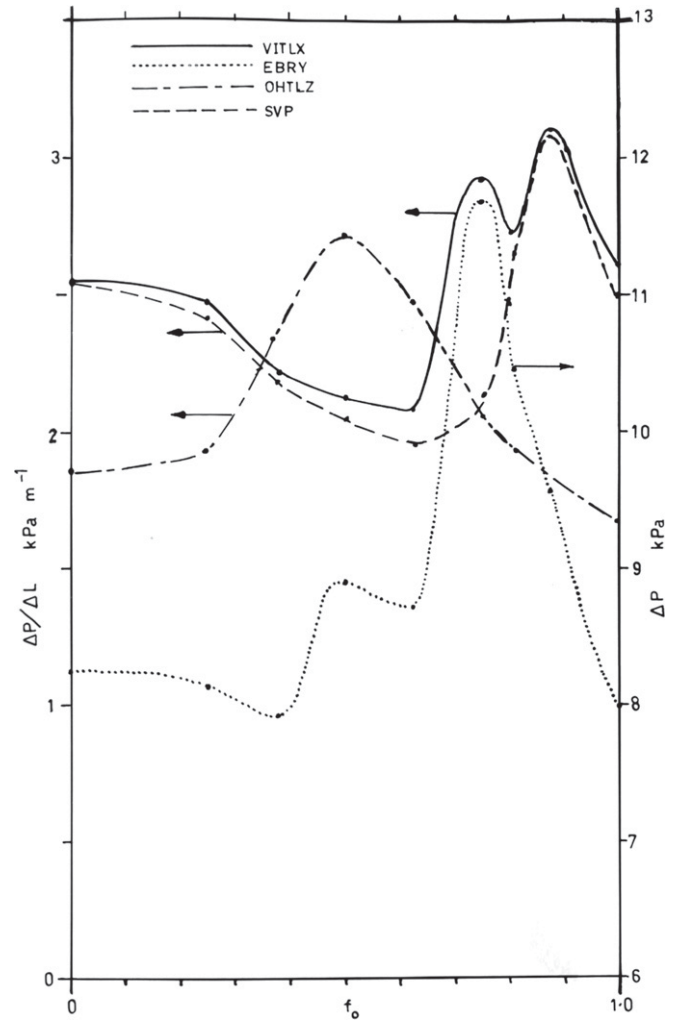


Fig. 8. Pressure losses through the vertical inlet tangent leg  $X$  (VITLX), straight vertical pipe (SVP), elbow bend region  $Y$  (EBRY), outlet horizontal tangent leg  $Z$  (OHTLZ) for  $\bar{V}_{SLT} = 0.1254 \text{ m s}^{-1}$  and  $\bar{V}_{SG} = 19.9 \text{ m s}^{-1}$ .

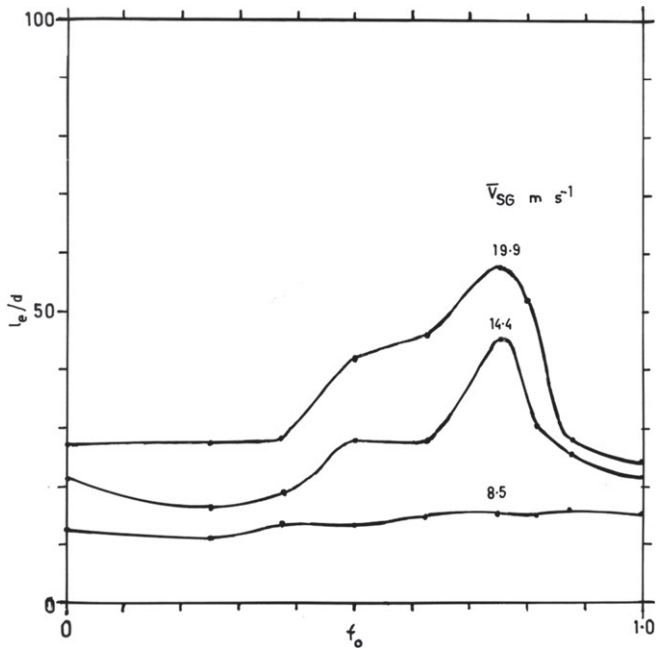


Fig. 7a. Bend pressure loss  $l_b/d$  for  $\bar{V}_{SLT} = 0.1254 \text{ m s}^{-1}$  and various gas rates.

appeared at  $f_o = 0.25$  as well as a larger one at  $f_o = 0.625$  (already noted in Fig. 3). Therefore, the flow patterns in the horizontal outward leg  $Z$  in Fig. 6 were more complex compared to the simple stratified regimes of Fig. 3. Donnelly [35] also observed the increased complexity of the flow patterns as the liquid rate rose. Eventually at the highest liquid flow rate in Fig. 9 droplets of oil were generated at  $f_o = 0.5$  creating a maximum in the pressure loss at this point. The subsequent fall in pressure loss from this maximum as the oil dominated region was approached reflected a fall in the oil to liquid ratio  $f_o$  in the body of the liquid phase.

As the liquid rate was increased further in Fig. 9 the effects shown in Fig. 6 were intensified. A comparison of settling lengths carried out by Donnelly et al. [35,36] for both three and two phase systems indicated that the settling length after the elbow bend used in this work was inadequate for three phase conditions at the higher flow rates. However, because the pressure drop in the



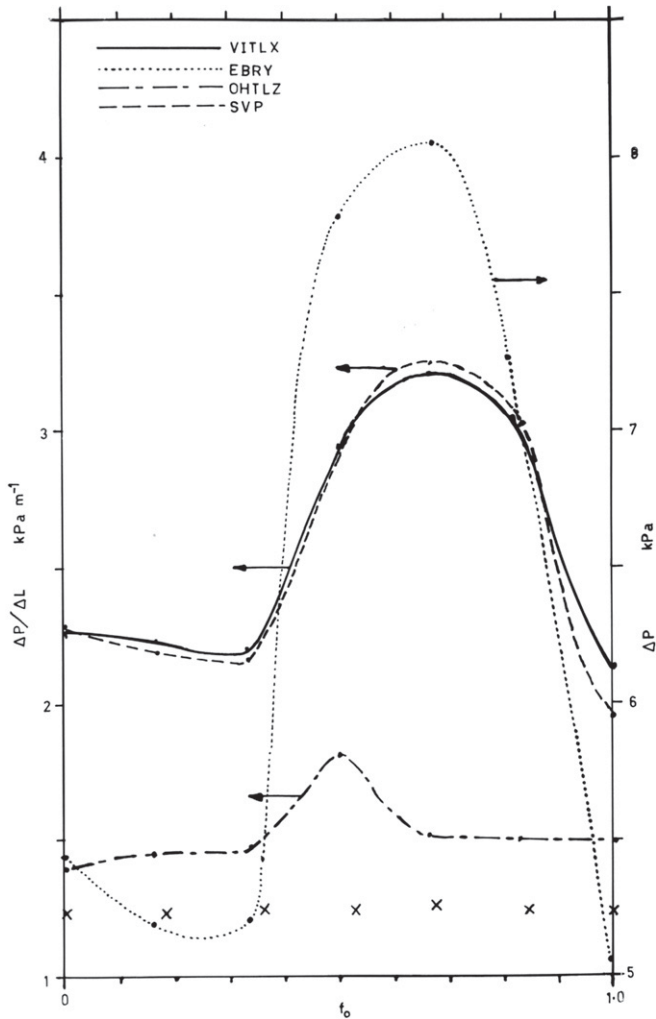


Fig. 9. Pressure losses through the vertical inlet tangent leg  $X$  (VITLX), straight vertical pipe (SVP), elbow bend region  $Y$  (EBRY), outlet horizontal tangent leg  $Z$  (OHTLZ) for  $\bar{V}_{SLT} = 0.1694 \text{ m s}^{-1}$  and  $\bar{V}_{SG} = 8.4 \text{ m s}^{-1}$ .  $X = \text{Donnelly [35] data}$ .

inlet vertical tangent leg  $X$  was so large a comparison of the data between two and three phase systems shows that the resulting error in the elbow bend pressure drop  $\Delta P_{TB}$  was no more than  $-5\%$ . Further, it was possible for the elbow bend to trigger the generation of a flow regime that remained permanently in the horizontal outlet tangent leg  $Z$  and not expected from a study of straight horizontal pipe three phase flow. This would be particularly the case under conditions close to the transition between water dominated and oil dominated flow.

Pressure drop in the elbow bend region  $Y$  tended to reflect the variation observed in the vertical inlet tangent leg  $X$ . The only exception was in Fig. 3 where the maximum pressure drop was at  $f_0 = 0.625$  for the elbow bend region  $Y$  and at  $f_0 = 0.75$  for the vertical inlet tangent leg  $X$ . The effect of the pressure drop in the horizontal outlet tangent leg  $Z$  appeared to have minimal effect on the elbow bend region  $Y$  pressure drop. The minimum point

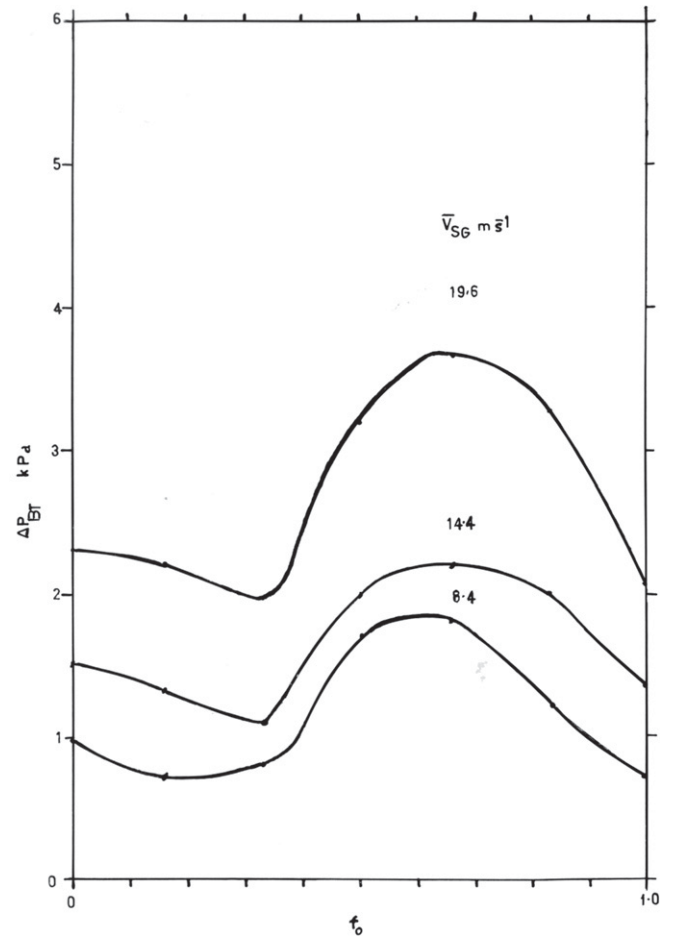


Fig. 9a. Bend pressure loss  $\Delta P_{BT}$  for  $\bar{V}_{SL} = 0.169 \text{ m s}^{-1}$  and various gas rates.

in the elbow bend region  $Y$  pressure drop fell from  $f_0 = 0.3$  to  $f_0 = 0.25$  as the liquid rate was increased. The position of the maximum point fluctuated from  $f_0 = 0.625$  to  $f_0 = 0.75$  and back to  $f_0 = 0.625$  as the liquid rate was increased. This effect was caused by different flow regimes being presented to the elbow bend and the increased pressure fluctuations at the  $f_0 = 0.625$  point.

The elbow bend pressure drop  $\Delta P_{BT}$  showed a very similar variation to the elbow bend region  $Y$  pressure drop in Figs. 3a, 6a and 9a. However, the  $l/d$  values of Figs. 4a, 7a and 10a were more constant. Fig. 4a showed a single maximum at  $f_0 = 0.625$  for all flow rates and a slight minimum at  $f_0 = 0.30$  for the highest gas rate. In addition the  $l/d$  values exhibited less variation over the range of variables that were used. The negative value in the elbow bend pressure drop observed in two phase flow at lower fluid flow rates was absent here [31].

When the gas rate was raised above  $\bar{V}_{SG} = 10 \text{ m s}^{-1}$  in the vertical inlet tangent leg  $X$  the general form of the various pressure drop relations altered significantly particularly for the vertical inlet tangent leg  $X$  (c.f. Figs. 4, 5, 7, 8 10 and 11). For the lowest total liquid superficial velocity

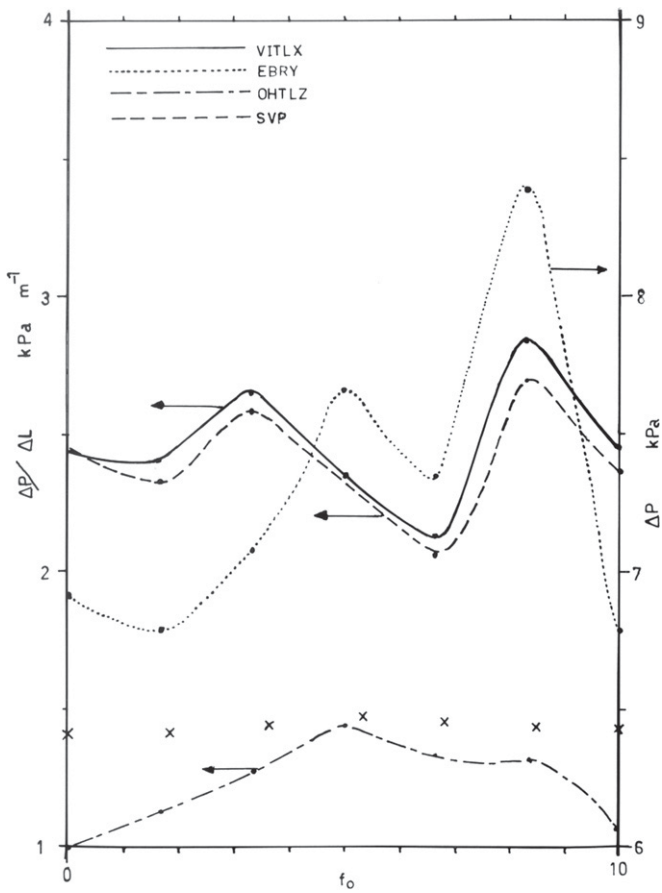


Fig. 10. Pressure losses through the vertical inlet tangent leg X (VITLX), straight vertical pipe (SVP), elbow bend region Y (EBRY), outlet horizontal tangent leg Z (OHTLZ) for  $\bar{V}_{SLT} = 0.1694 \text{ m s}^{-1}$  and  $\bar{V}_{SG} = 14.4 \text{ m s}^{-1}$ . X = Donnelly [35] data.

$\bar{V}_{SLT} = 0.063 \text{ m s}^{-1}$  shown in Figs. 4 and 5 the dip in the pressure loss relation for the vertical inlet tangent leg X at  $f_o = 0.625$  observed in Fig. 3, deepened to a substantial minimum. In Fig. 3 the water and oil dominated dispersed semi-annular regimes (No 5, No 20) formed over most of the  $f_o$  range with a tendency to form water dominated dispersed annulus/oil annular plus ripple flow (No 15) just before the start of inversion to oil dominated flow, whereas in Figs. 4 and 5 the water dominated dispersed annulus/oil annular plus ripple regime (No 15) was present well before inversion. Further, the maximum pressure loss in Figs. 4 and 5 was at  $f_o = 0.825$  where the oil dominated dispersed annular regime (No 2) was present, while in contrast the maximum was at  $f_o = 0.75$  in Fig. 3 in the oil dominated dispersed semi-annular regime (No 5) following inversion to oil dominated flow at  $f_o = 0.75$ . Thus all these differences can be attributed to differences in the flow regimes being present. In general the vertical inlet tangent leg X pressure drop followed the same form as the straight vertical pipe in Figs. 4 and 5 being above the latter at the extremities of  $f_o = 0$  and  $f_o = 1.0$  and below in the intermediate region i.e. the same as for Fig. 3.

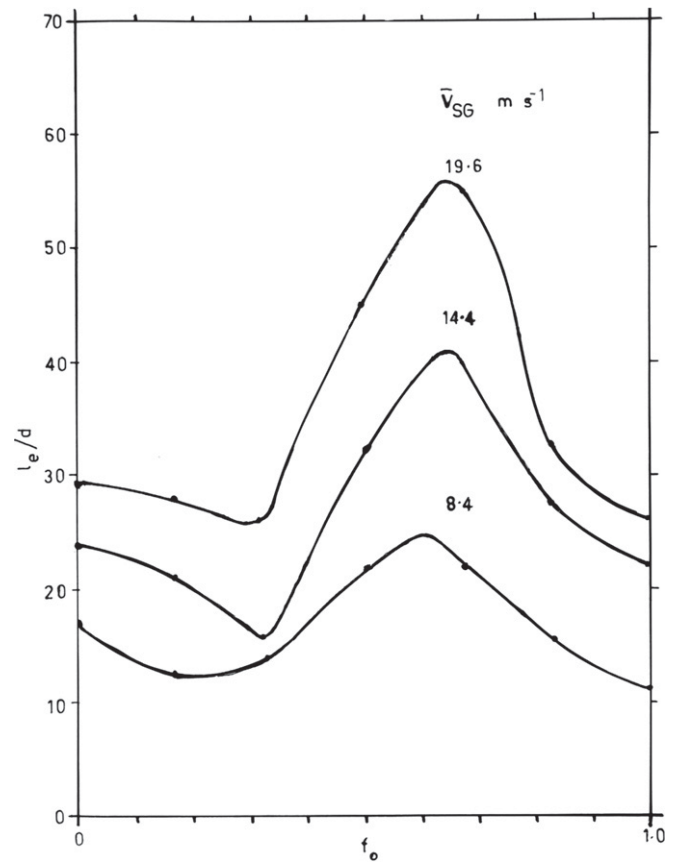


Fig. 10a. Bend pressure loss  $l_e/d$  for  $\bar{V}_{SL} = 0.1694 \text{ m s}^{-1}$  and various gas rates.

The pressure drop in the horizontal outlet tangent leg Z in Fig. 4 passed through a maximum at  $f_o = 0.675$  in a similar way to Fig. 3 except that at  $f_o = 0.675$  in Fig. 4 the oil phase was in slug flow. In addition the pressure losses in the horizontal outlet tangent leg Z in Figs. 4 and 5 were significantly above the data of Donnelly [35] and possessed much more complex stratified flow patterns. This was to be expected from the discussion of Fig. 9 already given before. At the highest gas rate in Fig. 5 the horizontal outlet tangent leg Z pressure drop was very different to those in Figs. 3 and 4 at the lower gas rates. Again the differences could be explained by altered flow regimes. At low oil to liquid ratios in Fig. 5 with  $f_o < 0.5$  the water dominated annular plus ripple flow regime was present. However, at  $f_o = 0.5$  slug flow developed in the water dominated regime, giving a maximum in the pressure drop relation. At  $f_o = 0.75$  the oil dominated regime did the same giving a second maximum. In between at  $f_o = 0.625$  a minimum was present in the oil dominated broken annular regime.

For Figs. 4 and 5 the elbow bend region Y pressure drop followed the same general form as the vertical inlet tangent leg Z pressure drop with little apparent influence from the horizontal outlet tangent leg Z. The elbow bend pressure drop  $\Delta P_{BT}$  was very different having a minimum

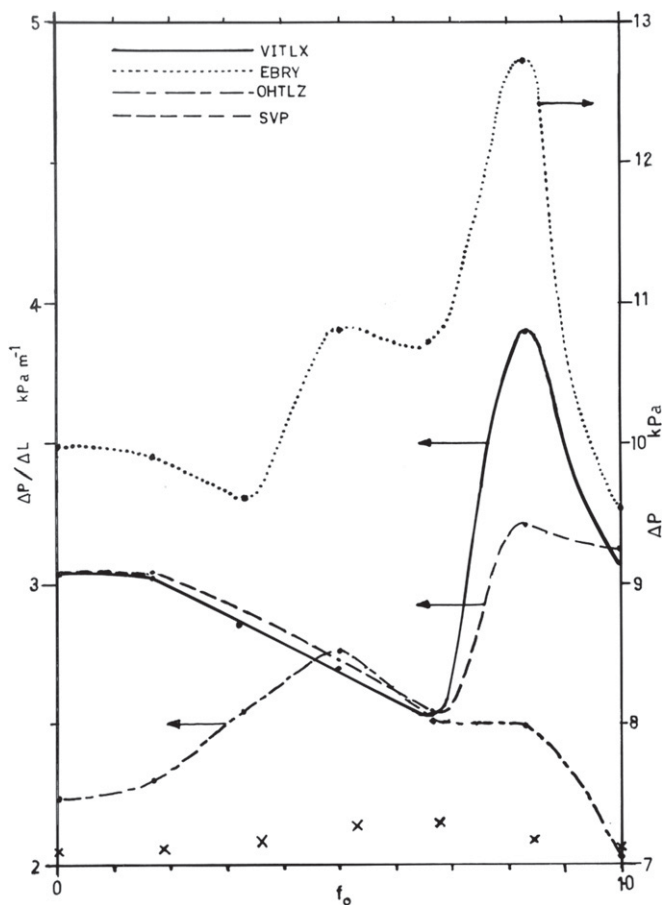


Fig. 11. Pressure losses through the apparatus, vertical inlet tangent leg  $X$  (VITLX), straight vertical pipe (SVP), elbow bend region  $Y$  (EBRY), outlet horizontal tangent leg  $Z$  (OHTLZ) for  $\bar{V}_{SLT} = 0.1694 \text{ m s}^{-1}$  and  $\bar{V}_{SG} = 19.6 \text{ m s}^{-1}$ .  $X$  = Donnelly [35] data.

and then a maximum  $f_o = 0.8$ . By contrast the  $l/d$  values gave a single maximum at  $f_o = 0.625$ , that was the same for all three gas rates at this lowest liquid rate (cf. Fig. 4a). This again shows the advantage of using  $l/d$  as a measure for the elbow bend pressure drop. When the liquid rate was doubled to  $\bar{V}_{SLT} = 0.125 \text{ m s}^{-1}$  for the two highest gas rates, as shown in Figs. 7 and 8, the vertical inlet tangent leg  $X$  pressure drop departed significantly from the general form for straight vertical pipe although the flow regimes remained visually the same. The vertical inlet tangent leg  $X$  values were above those for straight vertical pipe and possessed a double maxima. For  $\bar{V}_{SG} = 15.5 \text{ m s}^{-1}$  in Fig. 7 the maxima were at  $f_o = 0.375$  and  $f_o = 0.75$  while for  $\bar{V}_{SG} = 22.0 \text{ m s}^{-1}$  in Fig. 8 they were at  $f_o = 0.75$  and  $f_o = 0.875$ . In other aspects the pressure profiles in the vertical inlet tangent leg  $X$  and straight vertical pipe followed the same pattern. Woods et al. [27,28] studied three phase flow for straight vertical pipe and near vertical flow under identical conditions to those used in Figs. 7 and 8 in this work. They explained the significant differences observed between the two systems as being

caused by variations in the various holdup pattern profiles and in the fine structure of the flow regimes present. For example, the oil laminar to turbulent transitions as determined by reduction in pressure drop fluctuations, altered from  $f_o = 0.5$  for straight vertical pipe to  $f_o = 0.375$  for near vertical flow. No doubt a similar mechanisms could have caused the observed differences found between the vertical inlet tangent leg  $X$  and straight vertical pipe pressure drops observed in Figs. 7 and 8 in this work. However, further investigation is required before causes for these differences can be identified.

In Fig. 7 the horizontal outlet tangent leg  $Z$  pressure drop exhibited a single maximum at  $f_o = 0.625$  while in Fig. 8 at a higher gas rate the maximum was at  $f_o = 0.5$ . These maxima coincided with the point of inversion from water to oil dominated flows. At higher gas velocities in Fig. 8 the increased scouring of the water layer by the gas would result in the annular oil layer breaking through to the wall at an earlier point than experienced at the lower gas rate used in Fig. 7. The pressure drop in the horizontal outward leg  $Z$  in Fig. 8 was of a similar magnitude to that of the inlet vertical tangent leg  $X$ .

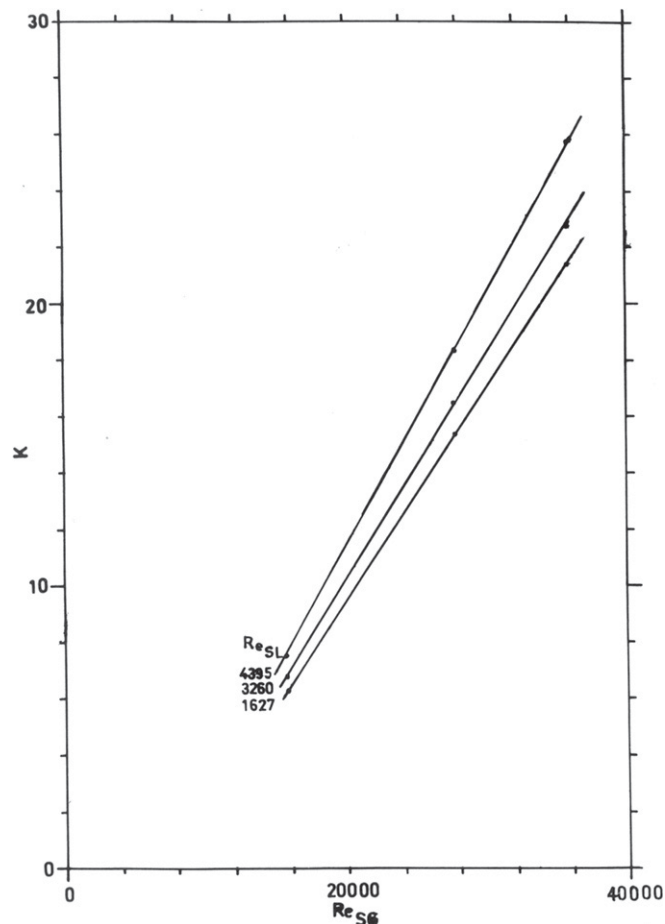


Fig. 12. Values of  $K$  in Eq. (1) for various values of phase Reynolds numbers.

The elbow bend region  $Y$  pressure drop followed the same general form as that observed for the vertical inlet tangent leg  $X$  in Fig. 7, but at the higher gas rate. In Fig. 8 a departure was observed that was traceable to the increased influence of the horizontal outlet tangent leg  $Z$  pressure drop. Indeed, it was possible that the increased influence of the pressure characteristics downstream of the elbow bend at this, the highest gas rate, may provide a valid explanation as to why the vertical inlet tangent leg  $X$  and straight vertical pipe pressure profiles were so different. Both the  $\Delta P_{BT}$  values of Fig. 6a and the  $l_e/d$  values of Fig. 7a show similar trends to the elbow bend region  $Y$  pressure drop with maxima at  $f_o = 0.75$ . The general form of these relations suggest that the  $l_e/d$  values tended to be the less variable parameters.

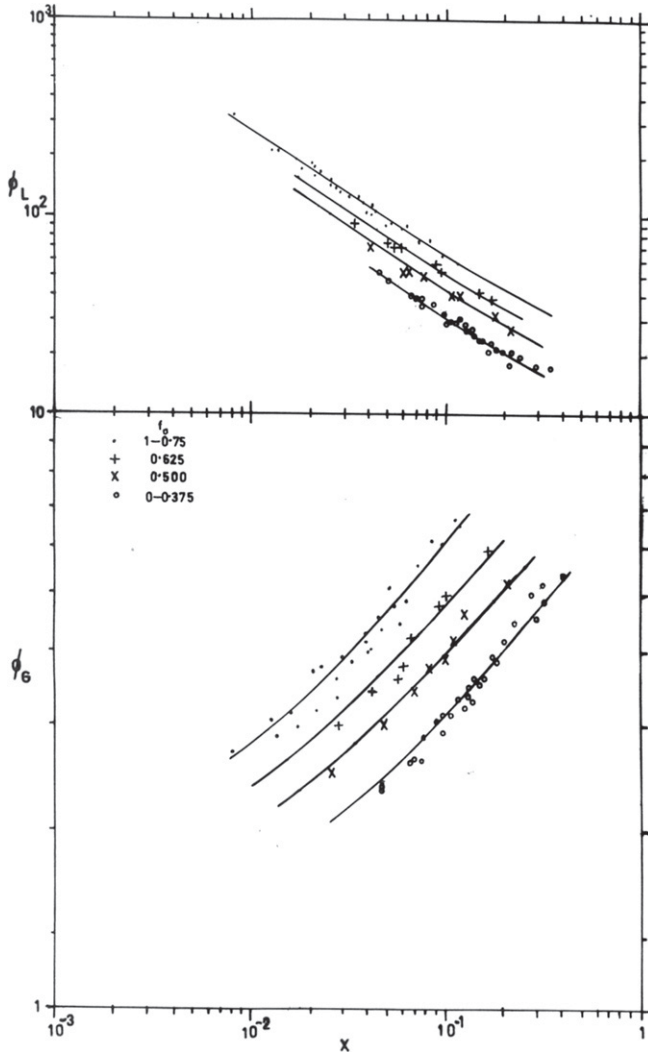


Fig. 13. The pressure drop in the form of the Lockhart-Martinelli parameters.

At the highest liquid rate of  $\bar{V}_{SLT} = 0.1694 \text{ m s}^{-1}$  and the two highest gas rates (cf. Figs. 10 and 11), the vertical inlet tangent leg  $X$  pressure drops showed similar trends to those observed in Figs. 7 and 8 but at a higher level. It should be noted that, particularly in Fig. 11, the wider intervals chosen in  $f_o$  values would have masked the lower of the double peak observed in the corresponding case of Fig. 8 at the lower total liquid rate. The data of Donnelly [35] show some measure of agreement with the horizontal outlet tangent leg  $Z$  pressure drop data of Fig. 10 but were below that for Fig. 11. Again, like in Fig. 3, the Donnelly [35] data did not exhibit the variation in either flow regimes or pressure drop found in this work. In Figs. 10 and 11 the horizontal outlet tangent leg  $Z$  pressure drop had maxima at  $f_o = 0.5$  where the annular droplet type regime occurred. Such a regime would be expected to exhibit a higher pressure drop since energy would be required to generate the droplets. The elbow bend region  $Y$  pressure profiles for Figs. 10 and 11 exhibited a double minimum/maximum characteristic similar to that found at lower total liquid rates (cf. Figs. 7 and 8).

Finally the  $\Delta P_{TB}$  data of Fig. 9a and the  $l_e/d$  values of Fig. 10a showed broad maxima at  $f_o = 0.67$  indicative of well mixed conditions.

When the  $f_o = 0$  values obtained in this work were compared to those for two phase air water flow [31] the  $l_e/d$  values obtained here were about 25% lower than the corresponding values obtained in the two phase experiments. The vertical inlet tangent leg  $X$  for the three phase experiment of this work were higher than the corresponding values obtained for the inlet tangent leg  $X$  in the two phase case. Since the pressure drop in the inlet tangent  $X$  was used to calculate  $l_e/d$  in each case then it would be expected that the higher inlet tangent pressure drop for three phase would result in a lower  $l_e/d$  value.

The data were correlated by the relation

$$l_e/d = A + K \exp[-B(f_o - 0.625)^2] \quad (1)$$

where

$$A = -1.465 \times 10^{-7} Re_{SL} Re_{SG} + 0.00179 Re_{SG} + 0.00614 Re_{SL} - 18.0 \quad (2)$$

$$B = 0.0008 Re_{SG} - 0.0029 Re_{SL} + 20.0 \quad (3)$$

and  $K$  is given by Fig. 12. Eq. (1) reproduced the results within +5% overall average.

Fig. 13 shows the data in the form of the Lockhart-Martinelli pressure loss parameter [32] using the actual single superficial phase pressure loss through the bend. Thus for gas flow

$$\phi_G = \left[ \frac{\Delta P_{BT}}{\Delta P_{BSG}} \right]^{0.5} \quad (4)$$

$$X = \left[ \frac{\Delta P_{BSL}}{\Delta P_{BSG}} \right]^{0.5} \quad (5)$$

The use of other correlating parameters such as the actual single superficial phase pressure losses in the tangent legs proved not to give acceptable correlations. The result emphasises the need to quantify the single phase effect of the bend pressure drop before proceeding to any multi-phase study.

The data of Fig. 13 fall into a series of four curves depending on  $f_o$  but not in a straight forward manner. The extremity curves at both low and high  $f_o$  values cover the range of  $f_o = 0-0.375$  and  $f_o = 0.75-1.0$ , respectively. However, in the intermediate region of  $f_o = 0.375-0.75$  there are individual relations for the variation of  $f_o$ . This is the region in which there are significant variations of viscosity as the composition of the liquid changes.

## 5. Conclusion

The results obtained were in general different if the superficial gas velocity was above or below  $\bar{V}_{SG} = 10 \text{ m s}^{-1}$ . In this the data followed effects observed in straight vertical pipe. For gas velocities  $\bar{V}_{SG} \leq 10 \text{ m s}^{-1}$  the pressure loss in the vertical inlet tangent leg  $X$  followed the same general form as that for straight vertical pipe being slightly above the straight vertical pipe data at the extremities around  $f_o = 0$  and  $1.0$  and below in the intermediate region. As the liquid rate was increased departure from the straight vertical pipe pressure drop pattern appeared due to differences in flow patterns between the two systems. Even the horizontal outlet tangent leg  $Z$  pressure drop was affected by the elbow bend, generally giving a higher pressure drop than straight pipe but also showed departures due to changes in the flow patterns between the two systems.

For gas velocities  $\bar{V}_{SG} \geq 10 \text{ m s}^{-1}$  at low liquid rates the vertical inlet tangent leg  $X$  pressure drop, while following the same general form as the straight vertical pipe data, were somewhat different to that for the  $\bar{V}_{SG} \leq 10 \text{ m s}^{-1}$  case. However, initially the vertical inlet tangent leg  $X$  pressure drop was still above the straight vertical pipe data at the extremities of  $f_o$  and  $f_o = 1.0$  below in the intermediate region. However, as the liquid rate was increased the pressure drop in the vertical inlet tangent leg  $X$  rose above the straight vertical pipe data in the intermediate regime, in some cases dramatically. The horizontal outlet tangent leg  $Z$  data showed similar dramatic differences to the straight pipe pressure loss. In most cases these departures from straight pipe data could be attributed to differences in flow regimes between the systems.

The elbow bend introduced a measure of choking of the flow in the vertical inlet tangent leg  $X$  and acted as a wave and droplet generator for the horizontal outlet tangent leg  $Z$ . Thus the pressure drop data for the tangent legs sometimes varied from that in straight pipe due in the main to changes in flow regimes. Further, work is required to determine if these effects are a permanent feature or if they could be eliminated by using longer settling lengths.

The elbow bend pressure drop was shown to be best represented by  $l_e/d$  using the actual pressure loss in the vertical inlet tangent leg  $X$  in the calculation. The value of  $l_e/d$  rose with gas rate at low liquid flows. A single maximum in  $l_e/d$  was in evidence at  $f_o = 0.625$ . As the liquid rate was increased the relationship with  $f_o$  became more complex eventually showing an additional minimum at lower  $f_o$  values.

Correlation of the data was achieved by two methods. One method used the Lockhart–Martinelli pressure parameter referred to the single phase pressure loss through the bend.

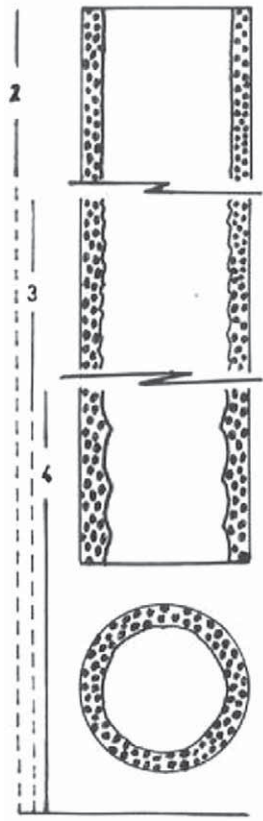
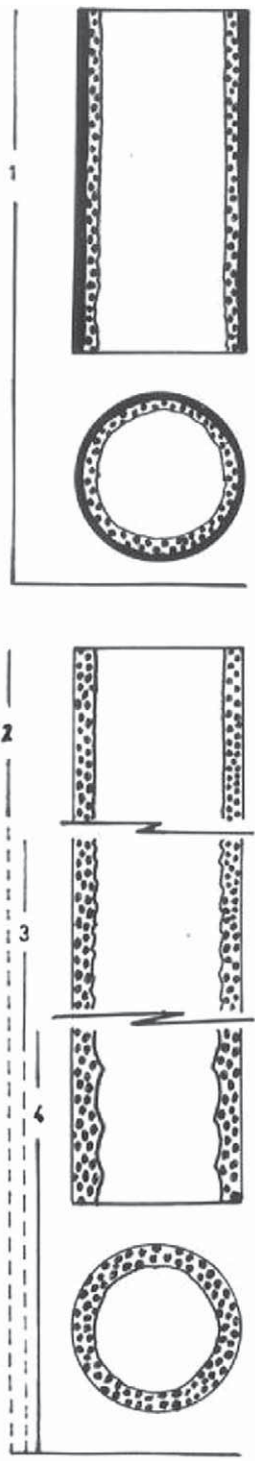
## Appendix

See Table 1.

Table 1  
Flow regimes in vertical three phase flow

Flow regime designation	Flow regime description
1	O.D. oil annulus/dispersed annular
2	O.D. dispersed annular
3	O.D. dispersed annular + ripple
4	O.D. dispersed annular + roll wave
5	O.D. dispersed semi-annular
6	O.D. dispersed semi-annular roll wave
7	O.D. dispersed churn
8	O.D. dispersed annular/dispersed slug
9	O.D. dispersed slug
10	O.D. broken annular
11	W.D. water annulus/oil annular
12	W.D. water annulus/oil annular + ripple
13	W.D. water annulus/oil annular + roll wave
14	W.D. dispersed annulus/oil annular
15	W.D. dispersed annulus/oil annular + ripple
16	W.D. dispersed annulus/oil annular + roll wave
17	W.D. dispersed annular
18	W.D. dispersed annular + ripple
19	W.D. dispersed annular + roll wave
20	W.D. dispersed semi-annular
21	W.D. dispersed semi-annular + ripple
22	W.D. dispersed semi-annular + roll wave
23	W.D. dispersed churn
24	W.D. dispersed annulus/dispersed slug
25	W.D. dispersed slug
26	W.D. oil slug







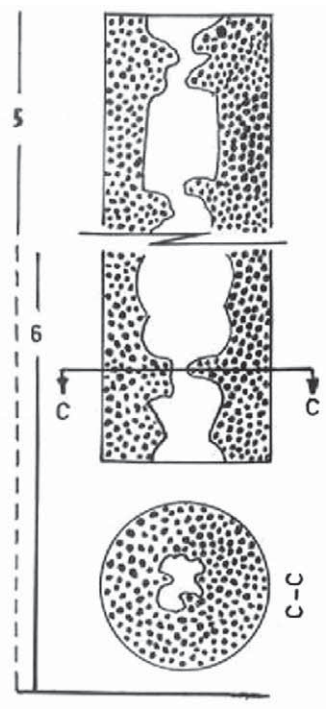


2

3

4

-  AIR
-  OIL
-  WATER IN OIL DISPERSION
-  WATER

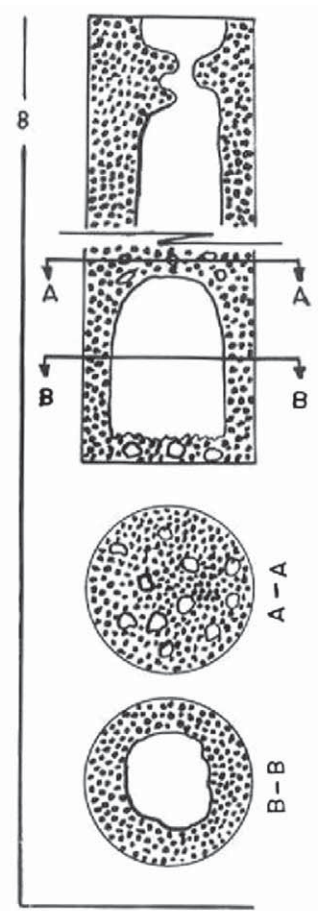


6

7

LIQUID MOTION

C-C



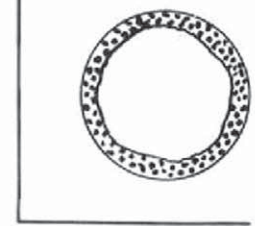
A

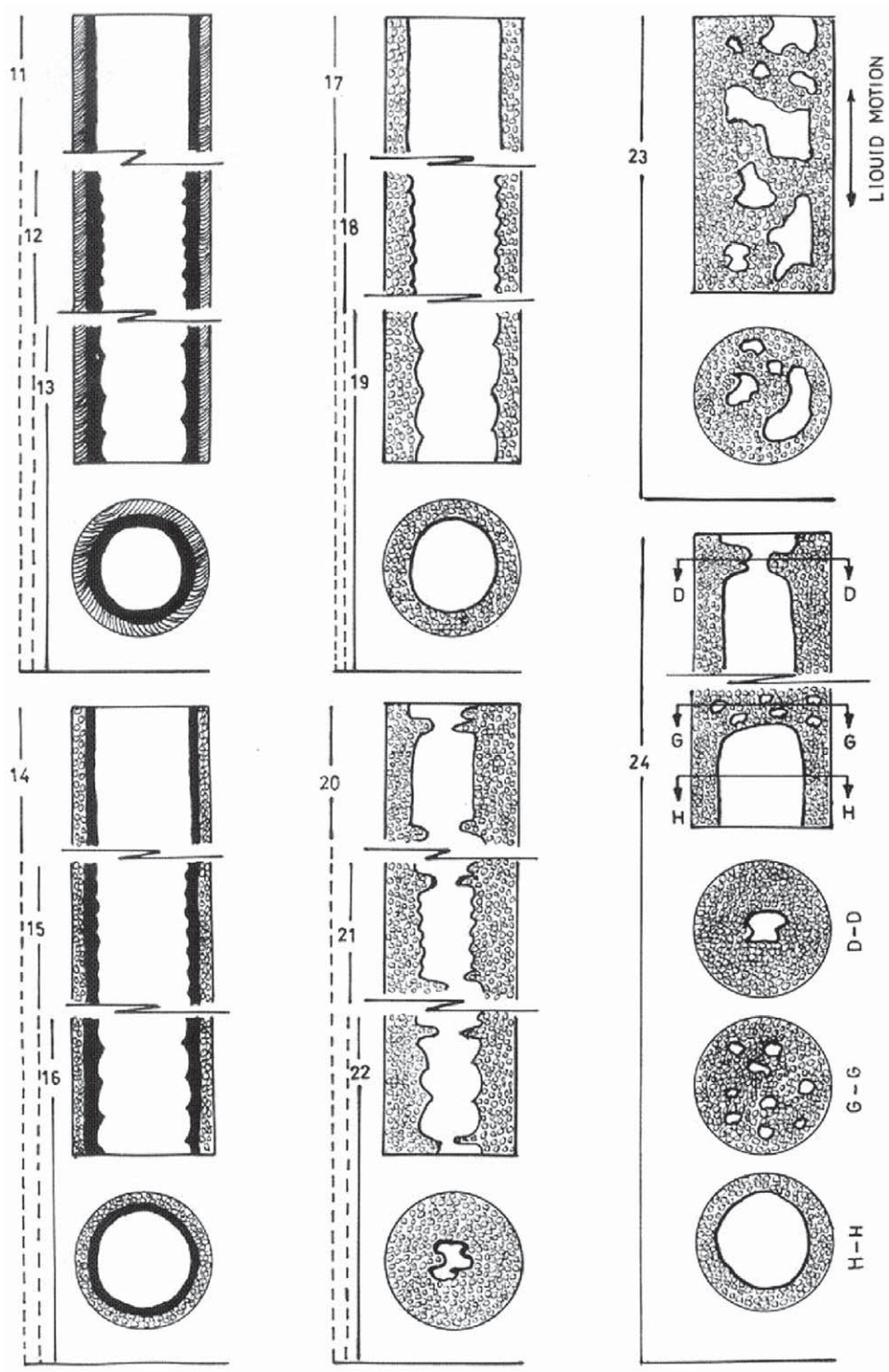
B

A-A

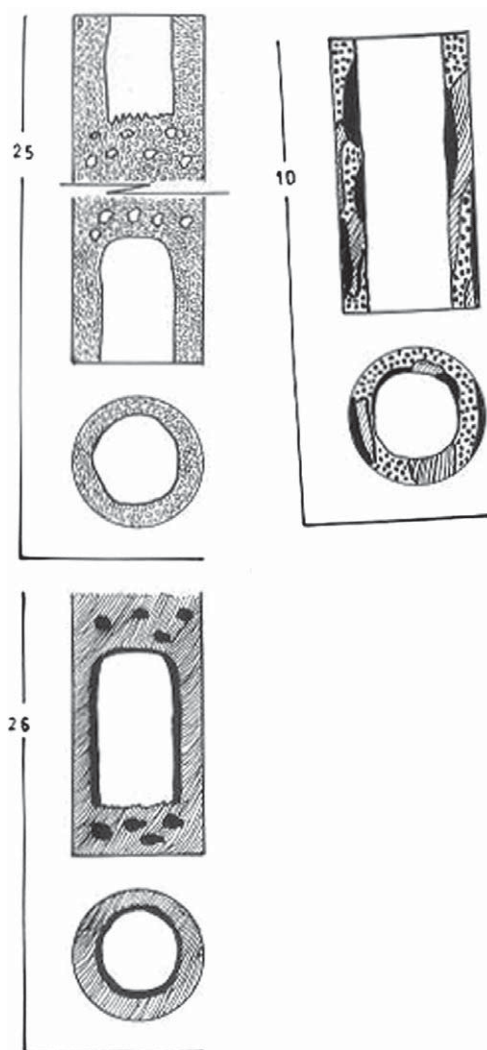
B-B

9





-  AIR
-  OIL
-  WATER
-  OIL IN WATER DISPERSION



## References

- [1] P.L. Spedding, G.F. Donnelly, J.S. Cole, Three phase oil–water–gas horizontal co-current flow. I Experimental and Regime map, *Trans. Inst. Chem. Eng.* 83A (2005) 401–411.
- [2] D.P. Sobocinski, R.L. Huntingdon, Co-current flow of air, gas–oil and water in a horizontal pipe, *Trans. ASME* 80 (1958) 252–256.
- [3] R.S. Shakirov, Pressure of hydraulic resistances during the motion of gas–oil–water mixtures in pipes, *Gazovoc Delo.* 11 (1969) 17–20.
- [4] P. Schlichting, The transport of oil–water–gas mixtures in oil field gathering systems, *Erdol-Erdgas-Zeitschrift* 86 (6) (1971) 235–249.
- [5] A.M. Bacharov, R.S. Andriasov, V.A. Sakharov, Investigation of the motion of gas, water, oil mixtures in horizontal pipe, *Nefte. Promyslovoe. Delo.* 6 (1972) 27–30.
- [6] A.I. Guzhov, V.F. Medverev, V.A. Savelev, Movement of gas–water–oil mixtures through pipelines, *Int. Chem. Eng.* 14 (1974) 713–714.
- [7] H. Stapelberg, D. Mewes, The flow of two immiscible liquids and air in a horizontal pipe, in: *ASME Proceedings of the Conference in Advances in Gas–Liquid flows*, FED 99 HTD 155 Dallas, Texas, 1990, pp. 89–96.
- [8] H. Stapelberg, D. Mewes, Three phase flow of oil, water and air in horizontal pipes, *VDI Forschungsheft.* 57 (668) (1991) 1–60.
- [9] M. Acikgoz, F. Franca, R.T. Lahey, An experimental study of three-phase flow regimes, *Int. J. Multiphase Flow* 18 (1992) 327–336.
- [10] R.T. Lahey, M. Acikgoz, F. Franca, Global volumetric phase fractions in horizontal three phase flow, *AICHE J.* 33 (1992) 1049–1058.
- [11] M. Nadler, D. Mewes, The effect of gas injection on the flow of immiscible liquids in horizontal pipes, in: *Proceedings of the German–Japanese Symposium Multiphase flow*, Karlsruhe, 1994, pp. 419–433.
- [12] M.S. Malinowsky, An experimental study of oil–water and air–oil–water flowing mixtures in horizontal pipes, M.Sc. thesis, University of Tulsa, 1975.
- [13] G.C. Lafin, K.D. Oglesby, An experimental study on the effects of flow rate, water fraction and gas liquid ratio on air–oil–water flow in horizontal pipes, B.Sc. thesis, University of Tulsa, 1976.
- [14] S. Nuland, K. Skavsvag, G. Seether, P. Fuchs, Phase fractions in three phase gas–oil–water flow, in: *Proceedings of the 5th International Conference Multiphase Production*, 1991, pp. 3–30.
- [15] H.A. Lee, J.Y. Sun, W.P. Jepson, Study of flow regime transitions of oil–water–gas mixture in horizontal pipelines, in: *Proceedings of the 3rd International Offshore and Polar Engineering Conference*, June 1993, pp. 159–164.
- [16] L. Pan, S. Jayanti, G.F. Hewitt, Flow patterns, phase inversion and pressure gradient in air–oil–water flow in a horizontal pipe, in: *Proceedings of the 2nd International Conference on Multiphase Flow*, Kyoto, Japan, 1995.
- [17] A.S. Fayed, L. Otten, Comparing measured with calculated multiphase flow pressure drop, *Oil Gas* (1983) 136–144.

- [18] Y. Taitel, D. Barnea, J.P. Brill, Stratified three phase flow in pipes, *Int. J. Multiphase Flow* 21 (1995) 53–60.
- [19] A.R.W. Hall, Multiphase flow of oil, water and gas in horizontal pipes, Ph.D thesis, Imperial College, 1992.
- [20] P.L. Spedding, E. Benard, G.F. Donnelly, Prediction of multiphase horizontal pipe flow: a reassessment. Part I: evaluation of two-phase correlations. Part II: pressure drop prediction in three-phase gas–oil–water flows, *Dev. Chem. Eng. Min. Process.* 14 (2006) 567–584.
- [21] F.H. Poettmann, P.G. Carpenter, The multiphase flow of gas, oil and water through vertical flow strings with application to design of air-lift installations, *API Drill* (1952) 257–317.
- [22] R.M. Tek, Multiphase flow of water, oil and natural gas through vertical flow strings, *J. Pet. Tech.* (1961) 1029–1036.
- [23] G.M. Francher, K.E. Brown, Prediction of pressure gradients for multiphase flow in tubing, *Soc. Pet. Eng. J.* (1963) 59–69.
- [24] A.R. Shean, Pressure drop and phase fraction in oil–water–air vertical pipe flow, M.Sc. thesis, M.I.T., 1976.
- [25] A. Pleshko, M.P. Sharma, An experimental study of vertical three phase (oil–water–air) upwards flow, in: *ASME Proceedings of the Conference Advances in gas–liquid flows*, FED 99 HTD 155 Dallas, 1990, pp. 81–88.
- [26] X.Z. Chen, X.J. Chen, F. Zhou, Phase holdups and frictional pressure gradient of oil–gas–water three phase bubbly flow in vertical upward pipes, in: *Sixth Miami International Symposium Heat Mass Transfer*, 1990.
- [27] G.S. Woods, P.L. Spedding, J.K. Watterson, S.R. Raghunathan, Three-phase oil/water/air vertical flow, *Trans. Inst. Chem. Eng.* 76A (1998) 571–584.
- [28] P.L. Spedding, G.S. Woods, S.R. Raghunathan, J.K. Watterson, Flow pattern, holdup and pressure drop in vertical and near vertical two and three-phase up flow, *Trans. Inst. Chem. Eng.* 78A (2000) 404–418.
- [29] H. Ito, Friction factors for turbulent flow in curved pipes, *Trans. ASME J. Basic Eng.* 81D (1959) 124–134.
- [30] N.M. Crawford, G. Cunningham, P.L. Spedding, Prediction of pressure drop for turbulent fluid flow in 90° bends, *Proc. Inst. Mech. Eng.* 217E (2003) 153–155.
- [31] P.L. Spedding, E. Benard, Gas–liquid two phase flow through a vertical 90° elbow bend, *Exp. Therm. Fluid Sci.* 31 (2007) 761–769.
- [32] R.W. Lockhart, R.C. Martinelli, Proposed correlation of data for isothermal two phase two component flow in pipes, *Chem. Eng. Prog.* 45 (1) (1949) 39–48.
- [33] P.L. Spedding, E. Benard, G.M. McNally, Fluid flow through 90° bends, *Dev. Chem. Eng. Mineral Process* 12 (2004) 107–128.
- [34] G.S. Woods, P.L. Spedding, Vertical, near vertical and horizontal co-current multiphase flow, Queen’s University Belfast, School Chemical Engineering, CE/96/Woods/2, 1996.
- [35] G.F. Donnelly, An analytical evaluation of horizontal multiphase flow, Ph.D thesis, Queen’s University, Belfast, 1997.
- [36] G.F. Donnelly, W.J. McBride, P.L. Spedding, Stable settling length for measurement of two phase air and water flow parameters, *Inst. Chem. Eng. Res. Event No 2* (1995) 820–822.